New Bandstop Filter Circuit Topology and Its Application to Design of a Bandstop-to-Bandpass Switchable Filter

Juseop Lee, *Member, IEEE*, Eric J. Naglich, *Student Member, IEEE*, Hjalti H. Sigmarsson, *Member, IEEE*, Dimitrios Peroulis, *Member, IEEE*, and William J. Chappell, *Senior Member, IEEE*

***Abstract*—In this paper, we show a new bandstop filter circuit topology. Unlike conventional bandstop filter circuit topologies, the new circuit topology has inter-resonator coupling structures. The presence of these inter-resonator coupling structures enables convenient switching from a bandstop to a bandpass filter. Using the new bandstop filter topology, this paper demonstrates a design of a frequency-agile bandstop-to-bandpass switchable filter. The filter is composed of tunable substrate-integrated cavity resonators and can be switched to have either a bandstop or bandpass response. Switching is achieved by turning on and off switches placed within the filter structure. A prototype of the proposed design is fabricated and the concept is verified experimentally.**

***Index Terms*—Bandpass filter, bandstop filter, filter synthesis, resonator filter.**

I. Introduction

As RF and microwave spectrum utilization grows, agile systems will continue to be a promising option for maintaining or improving the current capability of high-frequency devices [1]. One of the most challenging aspects of agile system design is adjustable filtering, due to difficult specifications concerning physical size, tuning range, and insertion loss, among other performance parameters. However, much progress has been made. Frequency tunable filters [2], [3], bandwidth tunable filters [4], and combinations of these capabilities [5]–[7] have been demonstrated. A filter structure with multiple functionalities, which can generate arbitrary-order filter responses, filter array responses, and switchable filter bank responses has also been recently reported [8]. In addition, intrinsically switched filters have also been reported [9].

Recently, the necessity and usefulness of the bandstop-to-bandpass reconfigurable filter from a system point of view were reported [10]. If multiple low-power interfering signals were in an open spectrum, the system could need a bandpass filter to isolate the signal of interest and maximize the signal-to-noise ratio (SNR). On the other hand, it could need a bandstop filter if an interferer close to the receive band existed. Bandstop-to-bandpass reconfigurable filters have the advantage of offering either an Nth-order bandpass response or an Nth-order bandstop response with only N resonators. In a crowded spectrum where both bandpass and bandstop filter responses could be needed at different times, these filters allow for a 50% reduction in filter volume because two different Nth-order filter responses can be obtained from N resonators. Past bandstop-to-bandpass filters have been designed with periodic structures [11] or with a maximum of two resonators [10], [12]. The current state-of-the-art does not include a methodology showing how to design higher order coupled-resonator bandstop-to-bandpass reconfigurable filters. This paper presents a rigorous extension of the bandstop-to-bandpass reconfigurable filter concept to an arbitrary filter order. As an example, this paper shows the design and measurement of a fourth-order bandstop-to-bandpass filter. For the design, we first developed a new bandstop filter topology, which has inter-resonator coupling structures. Due to the presence of the inter-resonator coupling structures, the bandstop filter can be conveniently switched to exhibit bandpass responses. A pair of switched conventional bandstop and bandpass filters (Fig. 1(a) can be replaced by the bandstop-to-bandpass reconfigurable filter [see Fig. 1(b)]). As the number of poles in a bandstop-to-bandpass reconfigurable filter grows, the volume reduction benefit increases. The capabilities of the proposed filter structure are expected to be useful in agile volume-constrained systems that will be operated in crowded spectral environments.

Manuscript received June 11, 2012; revised December 10, 2012; accepted December 10, 2012. Date of publication January 11, 2013; date of current version March 07, 2013. This work was supported by the Defense Advanced Research Projects Agency under the Purdue Evanescent-Mode Cavity Filter Study Program. The work of J. Lee was supported in part (since May 2012) by the Basic Science Research Program through the National Research Foundation of Korea (NRF) funded by the Ministry of Education, Science, and Technology (2012R1A1A1004665) .

J. Lee is with Department of Computer and Communications Engineering, Korea University, Seoul 136-701, Korea (e-mail: ifsnow@ieee.org).

E. J. Naglich, D. Peroulis, and W. J. Chappell are with the School of Electrical and Computer Engineering, Purdue University, West Lafayette, IN 47907 USA.

H. H. Sigmarsson is with the School of Electrical and Computer Engineering, University of Oklahoma, Norman, OK 73091USA.

Color versions of one or more of the figures in this paper are available online at http://ieeexplore.ieee.org.

Digital Object Identifier 10.1109/TMTT.2012.2237036

II. Design

A. Bandstop Filter Topology

Fig. 2(a) shows a low-pass circuit topology of a conventional fourth-order bandstop filter. S and L represent the source and load, and the numbers represent resonators. Each resonator is modeled as a unit capacitor in parallel with constant reactance $jM_{i,i}$ ($i = 1, 2, 3,$ and 4) to account for frequency shift of the resonant frequency. $N1$ and $N2$ are nonresonating nodes (NRNs), and each NRN is connected to the ground by a constant reactance jB_{Ni} ($i = 1$ and 2) [13]. All nodes (source,

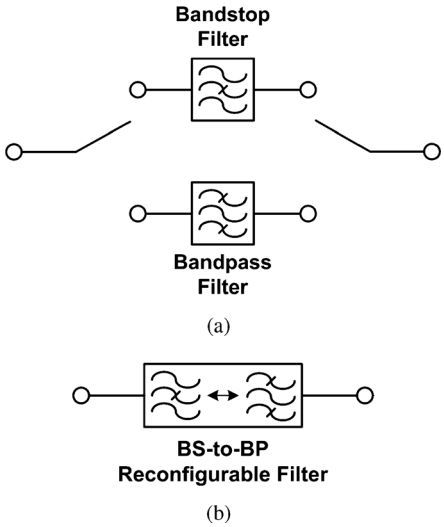

Fig. 1. (a) Pair of switched bandstop and bandpass filters. (b) Proposed circuit topology of fourth-order bandstop filter.

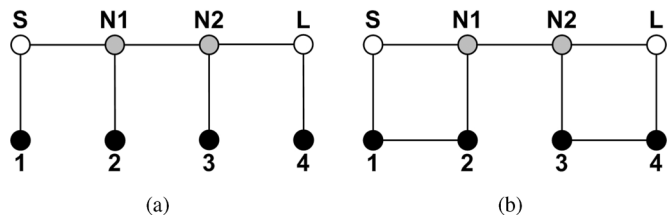

Fig. 2. Comparison of circuit topologies. The numbers represent resonators which can be any type such as lumped element resonator, microstrip line resonator, or cavity resonator. (a) Conventional circuit topology of fourth-order bandstop filter. (b) Proposed circuit topology of fourth-order bandstop filter.

load, resonators, and NRNs) are connected by admittance inverters whose values are represented by $M_{p,q}$ ($p, q = 1, 2, 3, 4$, $N1$, and $N2$).

Bandstop filters with the conventional circuit topology have a uniform transmission line between the source and load, and each resonator is coupled to the uniform transmission line [14]. However, the conventional bandstop filter cannot be easily switched to be a bandpass filter, due to the fact that there are no inter-resonator coupling structures. For the design of bandstop-to-bandpass switchable filters, we first developed a new circuit topology with inter-resonator coupling structures for bandstop filters. The new circuit topology is shown in Fig. 2(b), and its coupling matrix is shown in (1) at the bottom of this page. It is of note that the

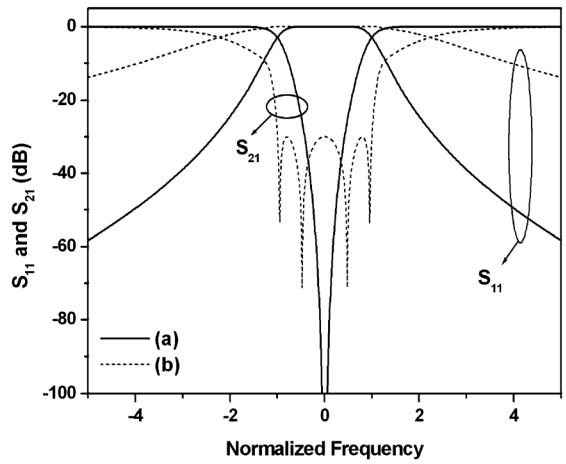

Fig. 3. (a) Frequency response of the filter with the coupling matrix given in (2). (b) Frequency response of the filter with the coupling matrix given in (3).

proposed circuit topology can be used for any type of resonators, such as a lumped-element resonator, microstrip line resonator, and cavity resonator. The coupling matrix for a prescribed frequency response can be obtained by using well-known filter synthesis methods [15]. For example, the solid lines in Fig. 3 show a fourth-order Butterworth bandstop response where all transmission zeros are at $S = 0$ (S: the normalized complex frequency), and all reflection zeros are at infinity in the normalized frequency domain, and the coupling coefficients are

$$\begin{aligned} M_{S,1} &= M_{4,L} = 1.359 \\ M_{1,2} &= M_{3,4} = 1.192 \\ M_{2,N1} &= M_{N2,3} = 0.877 \\ M_{S,N1} &= M_{N1,N2} = M_{N2,L} = 1.000 \\ M_{1,1} &= -M_{4,4} = 0.000 \\ M_{2,2} &= -M_{3,3} = 0.000. \end{aligned} \tag{2}$$

This frequency response can be obtained from the conventional bandstop filter topology [see Fig. 2(a)]. This indicates that the new bandstop filter topology can exhibit the frequency response that can be obtained from the conventional topology.

The dotted lines in Fig. 3 show another example of the bandstop response where transmission zeros are at $S = \pm j0.954$ and $\pm j0.478$ and refection zeros are at $S = -0.162 \pm j1.118$ and $\pm j\infty$. The reflection zeros are chosen arbitrarily for demonstration and the transmission zeros are determined in a way that

$$\mathbf{M} = \begin{bmatrix} 0 & M_{S,1} & 0 & M_{S,N1} & 0 & 0 & 0 & 0 \\ M_{S,1} & M_{1,1} & M_{1,2} & 0 & 0 & 0 & 0 & 0 \\ 0 & M_{1,2} & M_{2,2} & M_{2,N1} & 0 & 0 & 0 & 0 \\ M_{S,N1} & 0 & M_{2,N1} & 0 & M_{N1,N2} & 0 & 0 & 0 \\ 0 & 0 & 0 & M_{N1,N2} & 0 & M_{N2,3} & 0 & M_{N2,L} \\ 0 & 0 & 0 & 0 & M_{N2,3} & M_{3,3} & M_{3,4} & 0 \\ 0 & 0 & 0 & 0 & 0 & M_{3,4} & M_{4,4} & M_{4,L} \\ 0 & 0 & 0 & 0 & M_{N2,L} & 0 & M_{4,L} & 0 \end{bmatrix} \tag{1}$$

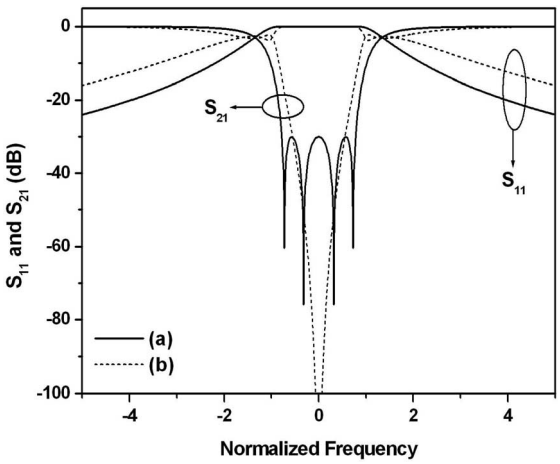

Fig. 4. (a) Frequency response of the filter with the coupling matrix given in (2) with $M_{i,i}$'s in (4). (b) Frequency response of the filter with the coupling matrix given in (3) with $M_{i,i}$'s in (5).

results in a 30-dB equi-ripple response in the stopband. Similarly, the coupling coefficients can be obtained and they are

$$\begin{aligned} M_{S,1} &= M_{4,L} = 1.567 \\ M_{1,2} &= M_{3,4} = 0.629 \\ M_{2,N1} &= M_{N2,3} = 1.053 \\ M_{S,N1} &= M_{N1,N2} = M_{N2,L} = 1.000 \\ M_{1,1} &= -M_{4,4} = 1.3126 \\ M_{2,2} &= -M_{3,3} = -0.8362. \end{aligned} \tag{3}$$

It is of note that the frequency response shown by dotted lines in Fig. 3 cannot be obtained from the conventional bandstop filter topology.

In new bandstop filter topology, $M_{1,2}$ and $M_{S,N1}$ have the same sign, and so do $M_{3,4}$ and $M_{N2,L}$. This allows a filter with the new bandstop filter topology to generate various kinds of frequency responses by detuning each resonator. In other words, the new topology allows for higher level flexibility with respect to varying the frequency response. For example, the frequency response plotted in solid lines shown in Fig. 4 can be obtained by simply changing the $M_{i,i}$'s ($i = 1, 2, 3,$ and 4) in (2) to

$$\begin{aligned} M_{1,1} &= -M_{4,4} = 0.728 \\ M_{2,2} &= -M_{3,3} = -0.321 \end{aligned} \tag{4}$$

and the one plotted in dotted lines shown in Fig. 4 can be obtained by changing the $M_{i,i}$'s ($i = 1, 2, 3,$ and 4) in (3) to

$$\begin{aligned} M_{1,1} &= -M_{4,4} = 0.802 \\ M_{2,2} &= -M_{3,3} = -0.800. \end{aligned} \tag{5}$$

It is worthwhile to note that detuning the resonant frequency of each resonator enables having different equi-ripple attenuation levels and bandwidths with no need of adjusting other coupling coefficients. In other words, having the same sign for $M_{1,2}$ and $M_{S,N1}$, and $M_{3,4}$ and $M_{N2,L}$ allows us to have either an equi-ripple response or a response with all transmission zeros at the same frequency by tuning each resonator. In addition, a bandstop filter with the new circuit topology has an advantage in terms of the capability of being switched to a bandpass filter due to the fact that it has inter-resonator coupling, which is indispensable to bandpass filter design. We will discuss how the bandstop filter with new topology can be switched to be a bandpass filter after discussing a physical design of the bandstop filter.

B. Physical Structure

In Section II-A, we proposed a new bandstop filter topology that has inter-resonator couplings. The presence of the inter-resonator couplings allows us to conveniently switch a bandstop filter to exhibit bandpass responses. This design approach can be used for any resonator structure. In this work, we chose high-Q tunable substrate-integrated cavity resonators for verifying the new bandstop filter topology shown in Fig. 2(b). Fig. 5 shows a 3-D drawing and simplified top- and side-view drawings of the bandstop filter with the new topology. In this work, high-Q tunable substrate-integrated cavity resonators are used. Four cylindrical cavity resonators are embedded in a 3.175-mm-thick Rogers TMM3 substrate ($\epsilon_r = 3.27$, $\tan\delta = 0.002$). The resonant frequency of the cavities is defined by the substrate height, the radius of the cage of via-holes forming the outer wall [r_1 in Fig. 5(b)], the radius of the central post, and the capacitive gap between the central post and copper membrane forming the bottom of the cavity. A 0.38-mm-thick commercially available piezoelectric actuator from Piezo Systems Inc., Woburn, MA, was attached under each cavity layer in order to control the gap by deforming the copper membrane. The via-holes in this design are 0.4 mm in radius and the post at the center of the cavity has a radius [r_3 in Fig. 5(b)] of 1.4 mm. An iris between two resonators forms the inter-resonator coupling structure, and its width [w in Fig. 5(b)] is determined by the required inter-resonator coupling coefficient. This iris is modeled as a shunt inductor between two resonators [16], which provides an approximate $+90^\circ$ phase shift.

Coupling structures between the source and the first resonator, between the first NRN and the second resonator, between the second NRN and the third resonator, and between the load and the fourth resonator were implemented by coupling slots in the copper layer beneath a 50-Ω microstrip transmission line fabricated on a 0.762-mm-thick Rogers 4350B substrate ($\epsilon_r = 3.48$, $\tan\delta = 0.0037$). The capacitive patches above the coupling slots are used to enhance the return loss in the passband [17]. The sizes of the coupling slots are determined by the coupling coefficients $k_{0,1}$, $k_{2,N1}$,$k_{N2,3}$, and $k_{4,L}$. The coupling coefficients are given by

$$k = \sqrt{\frac{\Delta f}{2}} M \tag{6}$$

where Δf is fractional bandwidth. In this work, we use the normalized coupling coefficients in (3) to obtain the frequency response in Fig. 3(b), and the design bandwidth was set to be 40 MHz at 2.7 GHz for this demonstration. Using full-wave simulations with the methodology described in [18], we obtained the coupling coefficient of the coupling slot. It is shown in Fig. 6(a) as a function of the sweep angle of the coupling slot given that the distance between the coupling slot and the center

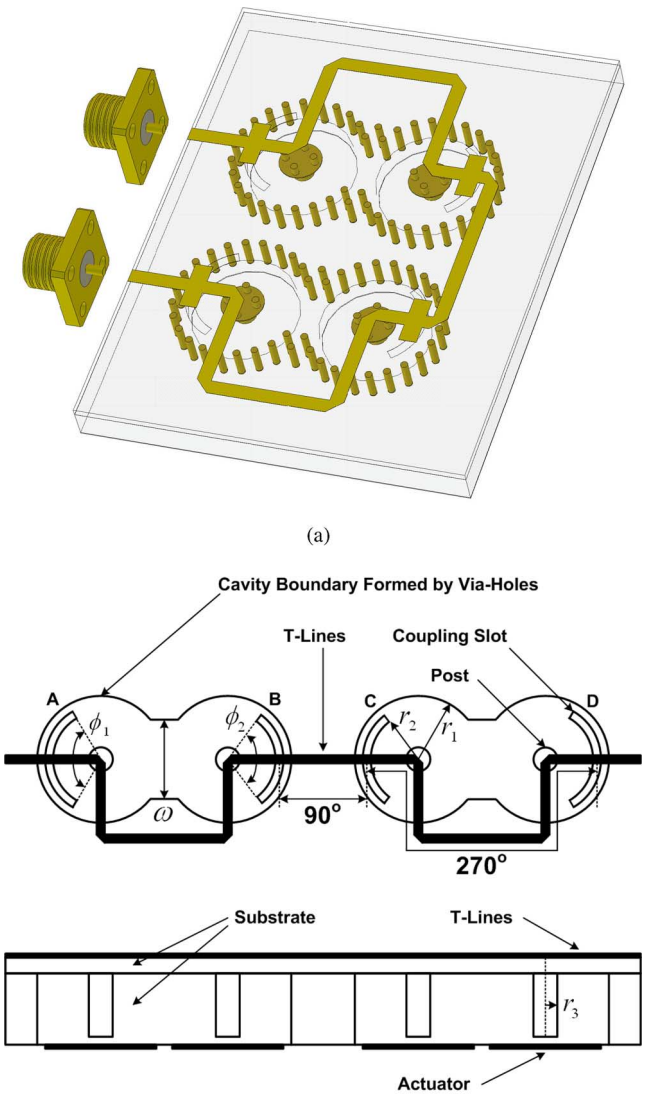

(a)

(b)

Fig. 5. (a) 3-D drawing of the bandstop filter. (b) Simplified top- and side-vide drawings ($\phi_1 = 128°$, $\phi_2 = 100°$, $w = 7.5$ mm, $r_1 = 7.5$ mm, $r_2 = 5.0$ mm, and $r_3 = 1.4$ mm).

of the cavity [r_2 in Fig. 5(b)] is 5.0 mm. The coupling coefficient increases as the sweep angle of the coupling slot increases. The sweep angles for the coupling slots, ϕ_1 and ϕ_2, are determined to be 128° and 100°, respectively. The electrical length between the coupling slots A and B and between coupling slots C and D were designed to be 270° at the design frequency, referenced from the middle of each coupling slot and including the phase from the inductive ground defect that the coupling slots impart. This line length is required to make $k_{S,N1}$, $k_{1,2}$, $k_{N2,L}$, and $k_{3,4}$ have the same sign.

Coupling structures between resonators 1 and 2 and between resonators 3 and 4 are formed by inductive irises. The coupling coefficient is mainly determined by the width of the iris [w in Fig. 5(b)], and it is summarized in Fig. 6(b). For an inter-resonator coupling structure, the coupling coefficient is given by

$$k = \Delta f \cdot M \tag{7}$$

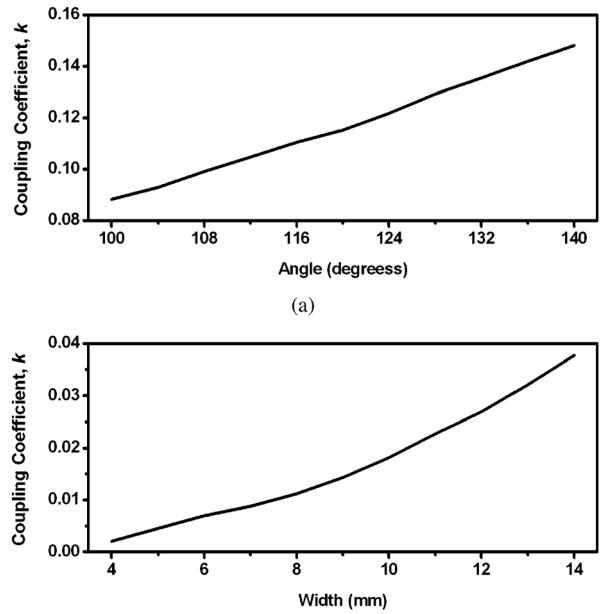

(a)

(b)

Fig. 6. (a) Coupling coefficient of the coupling slot between the transmission line and the resonator. (b) Coupling coefficient of the coupling iris between two resonators.

and the width of the iris has been designed to be 7.5 mm for the coupling coefficient needed in this work. All dimensions for the bandstop filter design are summarized in Fig. 5.

If we have an open circuit in each 270° transmission line, the filter can exhibit a bandpass filter response. This can be understood by contemplating a simplified drawing of the filter shown in Fig. 7. Input and output external coupling structures are formed by an open-circuited transmission line along with a coupling slot. Inter-resonator coupling structures between the first and second resonators and between the third and fourth resonators are also established by inductive irises. Lastly, an inter-resonator coupling structure between the second and third resonators is formed by two coupling slots and a transmission line with open ends on both sides. Therefore, this circuit is a direct-coupled resonator bandpass filter and its coupling matrix is given by

$$\mathbf{M} = \begin{bmatrix} 0 & M_{S,1} & 0 & 0 & 0 & 0 \\ M_{S,1} & 0 & M_{1,2} & 0 & 0 & 0 \\ 0 & M_{1,2} & 0 & M_{2,3} & 0 & 0 \\ 0 & 0 & M_{2,3} & 0 & M_{3,4} & 0 \\ 0 & 0 & 0 & M_{3,4} & 0 & M_{4,L} \\ 0 & 0 & 0 & 0 & M_{4,L} & 0 \end{bmatrix}. \tag{8}$$

The normalized coupling coefficients are determined by the prescribed frequency response. In this work, we design the filter in such a way that it can exhibit the frequency response shown in Fig. 8, and the normalized coupling coefficients are

$$\begin{aligned} M_{S,1} &= M_{4,L} = 1.009 \\ M_{1,2} &= M_{3,4} = 0.754 \\ M_{2,3} &= 0.541. \end{aligned} \tag{9}$$

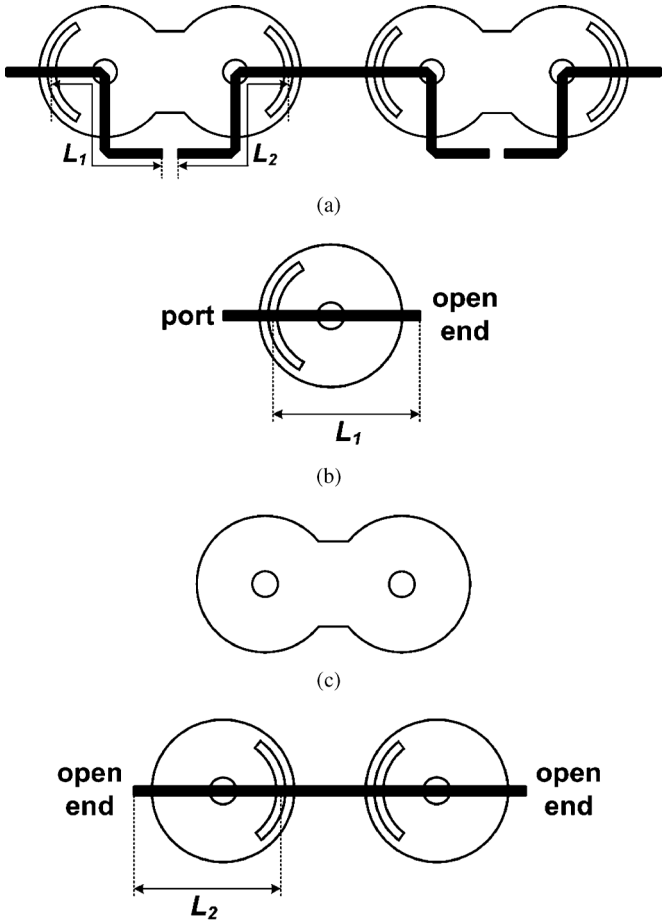

Fig. 7. (a) Simplified top-view drawing of the filter structure with open-circuits in the transmission line. (b) External coupling structure. (c) Inter-resonator coupling structure between resonators 1 and 2 and between resonators 3 and 4. (d) Inter-resonator coupling structure between resonators 2 and 3.

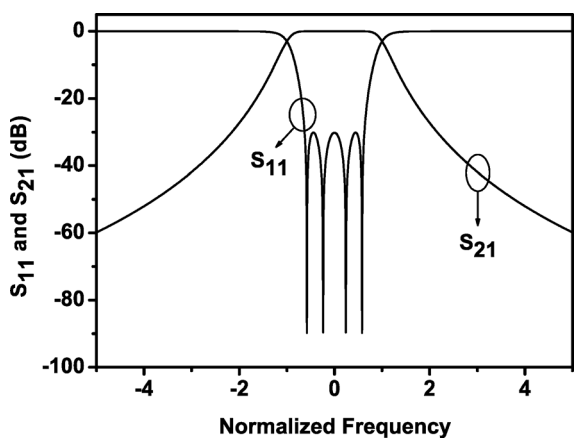

Fig. 8. Frequency response of the filter with coupling coefficients shown in (9).

The inter-resonator coupling structure formed by the inductive iris is used for generating both the bandstop response and the bandpass response. Therefore, the design bandwidth for the bandpass response is determined in such a way that the coupling coefficients of the inter-resonator coupling structure

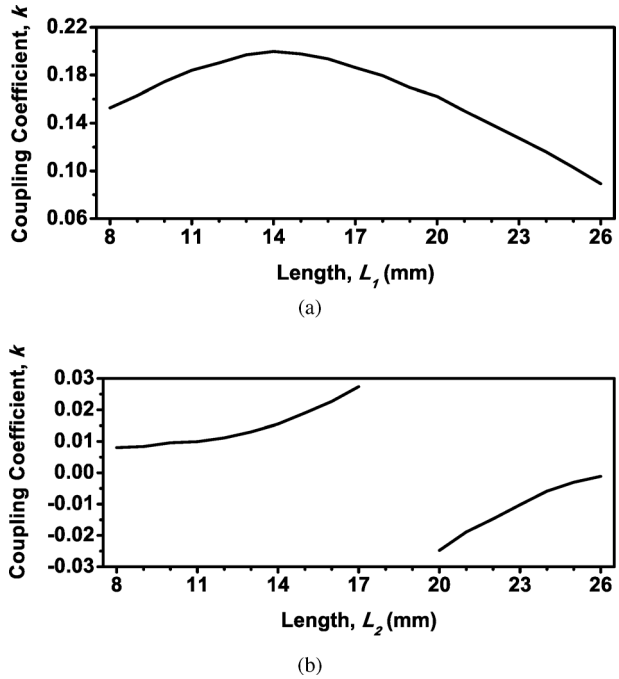

Fig. 9. (a) Coupling coefficient of the external coupling structure shown in Fig. 7(b). (b) Coupling coefficient of the inter-resonator coupling structure shown in Fig. 7(d).

for the bandstop response and bandpass response are identical. Therefore, the design bandwidth for the bandpass response is determined to be 33 MHz at 2.7 GHz for this demonstration. It is of note that the design bandwidth for the bandpass response can be made different by adjusting the coupling matrices for bandstop and bandpass responses. The coupling coefficient of the external coupling structure [see Fig. 7(b)] is controlled by the length of the open-circuited transmission line with the given size and location of the coupling slot. Using full-wave electromagnetic (EM) simulations, we extracted the coupling coefficient of the external coupling structure by following the methodology described in [19]. Fig. 9(a) shows the external coupling coefficient as a function of the length of the open-circuited transmission line. The length has been determined to be 24 mm using Fig. 9(a) and

$$k = \sqrt{\Delta f} M. \tag{10}$$

Since inductive coupling is dominant at the coupling slot, the coupling coefficient becomes maximum when the length of the open-circuited transmission line is close to a quarter-wavelength.

Similarly, with the given sizes of the coupling slots, the coupling coefficient between resonators 2 and 3 is determined by the transmission line length from the open end to the coupling slot (L_2), and this is summarized in Fig. 9(b). Fig. 9(b) shows that the inter-resonator coupling structure between resonators 2 and 3 can have either a positive or negative coupling coefficient depending on the length of the transmission line. This characteristic is described in [8], and it is not repeated in this paper. However, it is worthwhile to note that the sign of the coupling coefficient makes no difference in our case (direct-coupled

bandpass filter design) according to matrix similarity transformation theory [20]. Using Fig. 9(b), we can determine the length of the transmission line.

If the sum of L_1 and L_2 is equal to 270°, we need only one switch to replicate the open- and shorted-circuit in each of the 270° long transmission lines. This is a rare case, and two switches are theoretically needed to achieve the required dimensions: L_1 and L_2 for the bandpass response at turn-off state, and a 270° long transmission line for the bandstop response at turn-on state. However, a large number of switches results in a high insertion loss. In the case where the bandstop filter can tolerate the fact that the transmission lines between coupling slots A and B and between coupling slots C and D are not 270° long, but close to it, we can use one switch in each of those transmission lines. Therefore, we put one switch in each of those transmission lines.

With an open circuit in each of the transmission lines between coupling slots A and B and between coupling slots C and D, we can have inter-resonator coupling between neighboring resonators. In other words, coupling structures can be established between consecutively numbered resonators, which is indispensable for designing direct-coupled bandspass filters. Therefore, we can design a reconfigurable filter that can be switched to have either a bandpass or a bandstop response. In order to have the capability of having a short circuit and an open circuit in each of those transmission lines, we employ reflective microelectromechanical systems (MEMS) switches from Omron, Kyoto, Japan (part #: 2SMES-01). Isolation, insertion loss, and return loss are 30, 1, and 10 dB up to 10 GHz, respectively. At off-state, the switch has parasitic capacitance, which causes a nonzero phase shift. The phase shift has been measured for the individual MEMS switches. Due to this phase shift, the microstrip-line structure shown in Fig. 5(a) has been modified to absorb the phase shift generated by the MEMS switches, and the physical structure of the bandstop-to-bandpass switchable filter is shown in Fig. 10.

In summary, the design procedure for the reconfigurable filter is as follows.

1) Define the fractional bandwidths and frequency responses for the bandstop and bandpass states.
2) Obtain the coupling matrices for bandstop and bandpass responses (If the coupling matrices do not allow for sharing the coupling irises, go back to 1) and adjust the frequency responses).
3) Design the coupling slots and irises using (6) and (7).
4) Find L_1 and L_2 for finding the location of the switches using the design graphs shown in Fig. 9.

III. Measurements

A prototype of the filter structure described in Section II was fabricated, and the measured results are shown in the subsequent figures. First, the switches were turned on to have bandstop responses, and Fig. 11 shows the measured frequency responses. The filter can be continuously tuned from 2.7 to 3.0 GHz. Frequency tuning is achieved by changing the thickness of the air gap between the post and the bottom conductor layer. The thickness of the air gap is adjusted by a piezoelectric actuator (Piezo Systems Inc., Woburn, MA T216-A4NO-273X), which is attached to the bottom conductor layer. DC voltage from −200 to +200 V can be applied to the piezoelectric actuators for frequency tuning, and higher voltage results in a lower filter center frequency. The measured 30-dB-rejection bandwidth is 37.5 MHz, 41.5, 42.5, and 42.5 MHz at 2.7, 2.8, 2.9, and 3.0 GHz, respectively. The passband insertion loss of the filter responses, including the loss of connectors at the ports and the MEMS switches, is 1.2 and 2.0 dB at 2.5 and 3.2 GHz, respectively. The filter has higher insertion loss at higher frequencies mainly due to the fact that the insertion loss of the MEMS switch increases as the frequency increases. For the bandstop response, the signal passes through the two on-state switches in the reconfigurable filter [see Fig. 1(b)] and in the conventional configuration [see Fig. 1(a)]. Therefore, the insertion loss of the reconfigurable filter is theoretically identical to that of the bandstop filter in the conventional configuration. Since the MEMS switches and the printed circuit board (PCB) pads for them do not provide the perfect 50-Ω matching, the reflection coefficients of the responses start to be worse than −10 dB at 3.9 GHz. This passband matching performance can be improved by more careful design of PCB pads for the MEMS switches.

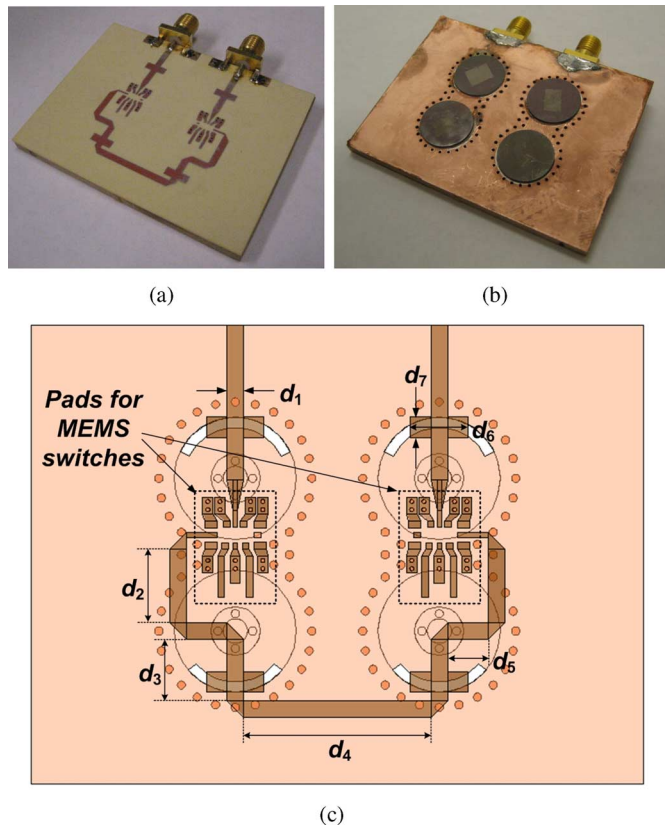

Fig. 10. (a) Photograph of the front side of the fabricated filter (switches are not shown in order to show the pads for MEMS switches). (b) Photograph of the back side of the fabricated filter. (c) Top-view drawing of the fabricated filter with dimensions ($d_1 = 1.640$ mm, $d_2 = 7.185$ mm, $d_3 = 6.000$ mm, $d_4 = 18.360$ mm, $d_5 = 4.000$ mm, $d_6 = 5.640$ mm, and $d_7 = 2.000$ mm).

As discussed in Section II, the new circuit topology allows us to have different bandstop filter responses by adjusting the resonant frequency of each resonator. For example, the bandstop filter can create a deep notch by adjusting the resonant frequency

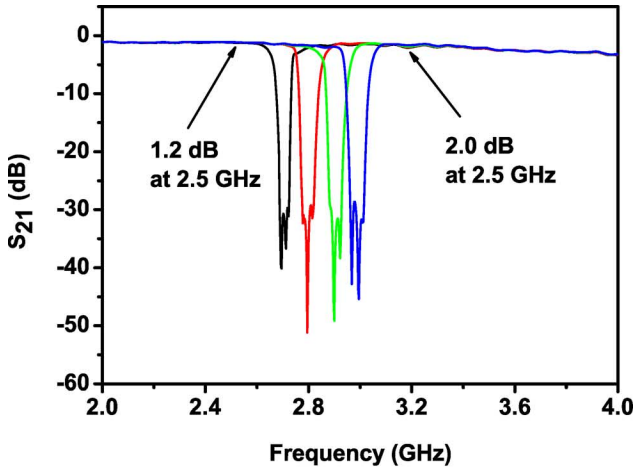

(a)

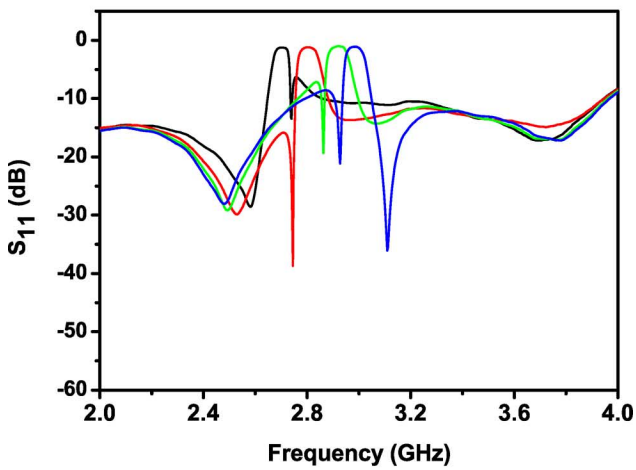

(b)

Fig. 11. Measured frequency response of the filter. The 30-dB equi-ripple bandstop responses are shown. (a) Transmission coefficient. (b) Reflection coefficient.

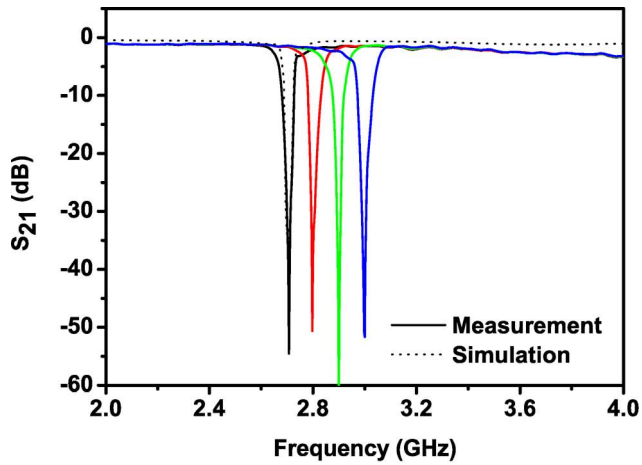

(a)

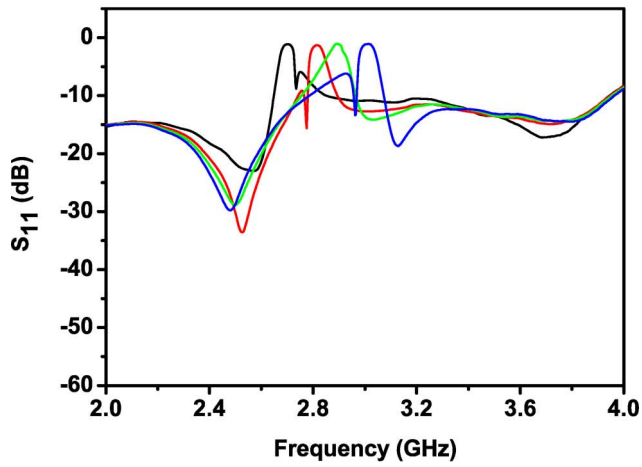

(b)

Fig. 12. Measured frequency response of the filter. The bandstop filter is tuned to have all transmission zeros at the same frequency for each response. (a) Transmission coefficient. (b) Reflection coefficient.

of each resonator. In order to verify this concept, the filter has been tuned in such a way that it creates a single deep notch by having all transmission zeros at the same frequency, and the measured result is shown in Fig. 12. All transmission zeros are located at the same frequency, which results in a narrow bandwidth. This verifies that the filter with the new topology can generate different attenuation levels and bandwidths by tuning each resonator.

The filter can be switched to exhibit bandpass responses by turning off the MEMS switches, and Fig. 13 shows the measured results of the filter. Although the physical dimensions of the filter are determined by full-wave EM simulations targeting 2.7 GHz, bandpass response can also be tuned from 2.7 to 3.0 GHz. The measured and simulated 3-dB bandwidths are 25 and 23.5 MHz, respectively. The measured insertion loss in the passband is 4.7, 4.8, 5.1, and 6.0 dB when the filter is centered at 2.7, 2.8, 2.9, and 3.0 GHz, respectively. In this work, the design bandwidth for the bandpass response has been set to be smaller than that for the bandstop response. Since the insertion loss of the bandpass response is inversely proportional to the bandwidth and the Q factor of the resonators, having smaller bandwidth results in larger insertion loss. Although the Q factor of each resonator is high $(Q > 500)$, moderate insertion loss is observed, which is mainly attributed to the narrow design bandwidth of the filter. The insertion-loss performance can be improved by further enhancing the Q factor of each resonator. The switches are embedded in the reconfigurable filter and the MEMS switches have little influence on the insertion loss of the bandpass responses theoretically. This is because the signal does not pass through the off-state switches for the bandpass mode. On the other hand, the insertion losses of the two switches are directly added to the insertion loss of the bandpass filter in the conventional configuration [see Fig. 1(a)] since the signal passes through the two switches. Therefore, the insertion loss of the reconfigurable filter for the bandpass state is theoretically smaller than that of the bandpass filter in the conventional configuration. Small discrepancy between the simulation and measurement can be attributed to fabrication tolerances and the high sensitivity of the frequency tuning due to the narrow bandwidth. In addition, it is possible that each switch has different parasitics, which play an important role in determining the length of the microstrip transmission lines. The transmission zeros in

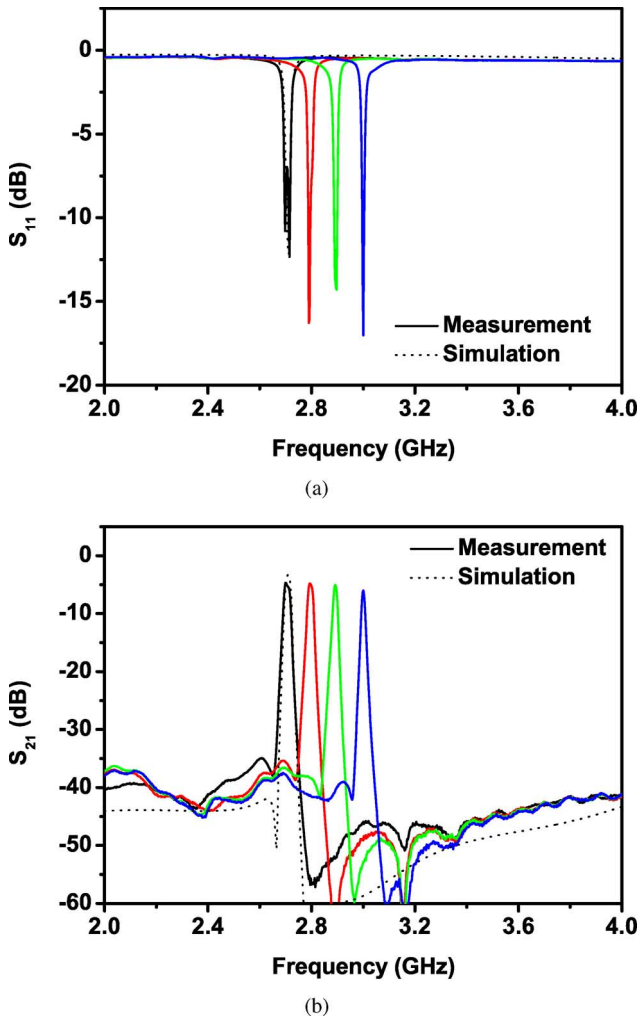

Fig. 13. Measured frequency response of the filter. The filter is switched to have bandpass responses at different center frequencies. (a) Transmission coefficient. (b) Reflection coefficient.

each side of the stopband can be attributed to the nonzero coupling between the source and load through the transmission line and the MEMS switches. The out-of-band isolation is around 35–40 dB. It is mainly due to the limited isolation performance of the MEMS switches. The out-of-band isolation performance can be improved by enhancing the isolation performance of the MEMS switches for the off-state.

The reconfigurable filter in this work can be tuned from 2.7 to 3.0 GHz with good bandstop and bandpass responses. The frequency tuning range is mainly limited by the fact that the coupling coefficient of each coupling structure varies with the frequency. Therefore, the frequency tuning range can be increased by employing tunable coupling structures.

It has been shown that we can design bandstop-to-bandpass switchable filters by using the proposed bandstop filter topology with inter-resonator coupling structures. These inter-resonator coupling structures allow us to conveniently reconfigure the filter structure using switches. This approach can also be applied to higher even-number-order reconfigurable filter design, and Fig. 14 shows a sixth-order bandstop filter topology with inter-resonator coupling structures as an example. Future research

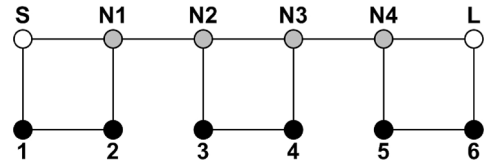

Fig. 14. Sixth-order bandstop filter topology with inter-resonator coupling structures.

may include development of the topology for odd-number-order filters.

IV. Conclusion

In this paper, we have presented a new bandstop filter topology with inter-resonator coupling structures. We have shown that the bandstop filter with the new topology can be conveniently switched to have a bandpass response due to the presence of the inter-resonator coupling structures. In order to verify the new topology, a switchable filter with a tuning range from 2.7 to 3.0 GHz was designed using tunable substrate-integrated-waveguide resonators. The filter was reconfigured by a pair of reflective MEMS switches, and it was demonstrated that the switchable filter can exhibit both bandstop and bandpass filter responses with good agreement between simulations and measurements. Filter with these capabilities can offer a significant improvement to reconfigurable front-end transceivers as they provide tailored transfer functions for a wide range of spectral environments.

References

[1] S. Geirhofer, T. Lang, and B. M. Sadler, "Cognitive radios for dynamic spectrum access-dynamic spectrum access in the time domain: Modeling and exploiting white space," *IEEE Commun. Mag.*, vol. 45, no. 5, pp. 66–72, May 2007.

[2] R. M. Young, J. D. Adam, C. R. Vale, T. T. Braggins, S. V. Krishnaswamy, C. E. Milton, D. W. Bever, L. G. Chorosinski, L.-S. Chen, D. E. Crockett, C. B. Freidhoff, S. H. Talisa, E. Capelle, R. Tranchini, J. R. Fende, J. M. Lorthioir, and A. R. Tories, "Low-loss bandpass RF filter using MEMS capacitance switches to achieve a one-octave tuning range and independently variable bandwidth," in *IEEE MTT-S Int. Microw. Symp. Dig.*, Philadelphia, PA, 2003, pp. 1781–1784.

[3] S. Moon, H. H. Sigmarsson, H. Joshi, and W. J. Chappell, "Substrate integrated evanescent-mode cavity filter with a 3.5 to 1 tuning ratio," *IEEE Microw. Wireless Compon. Lett.*, vol. 20, no. 8, pp. 450–452, Aug. 2010.

[4] C. Rauscher, "Reconfigurable bandpass filter with a three-to-one switchable passband width," *IEEE Trans. Microw. Theory Techn.*, vol. 51, no. 2, pp. 573–577, Feb. 2003.

[5] M. Sánchez-Renedo, R. Gómez-García, J. I. Alonso, and C. Briso-Rogríguez, "Tunable combline filter with continuous control of center frequency and bandwidth," *IEEE Trans. Microw. Theory Techn.*, vol. 53, no. 1, pp. 191–199, Jan. 2005.

[6] H. Joshi, H. H. Sigmarsson, S. Moon, D. Peroulis, and W. J. Chappell, "High-Q fully reconfigurable tunable bandpass filters," *IEEE Trans. Microw. Theory Techn.*, vol. 57, no. 12, pp. 3525–3533, Dec. 2009.

[7] C.-C. Cheng and G. M. Rebeiz, "High-Q 4–6 GHz suspended stipline RF MEMS tunable filter with bandwidth control," *IEEE Trans. Microw. Theory Techn.*, vol. 59, no. 10, pp. 2469–2476, Oct. 2011.

[8] J. Lee, E. J. Naglich, H. H. Sigmarsson, D. Peroulis, and W. J. Chappell, "Tunable inter-resonator coupling structure with positive and negative values and its application to the field-programmable filter array (FPFA)," *IEEE Trans. Microw. Theory Techn.*, vol. 59, no. 12, pp. 3389–3400, Dec. 2011.

[9] A. C. Guyette, "Intrinsically switched varactor-tuned filters and filter banks," *IEEE Trans. Microw. Theory Techn.*, vol. 60, no. 4, pp. 1044–1056, Apr. 2012.
[10] E. J. Naglich, J. Lee, D. Peroulis, and W. J. Chappell, "A tunable bandpass-to-bandstop reconfigurable filter with independent bandwidths and tunable response shape," *IEEE Trans. Microw. Theory Techn.*, vol. 58, no. 12, pp. 3770–3779, Dec. 2010.
[11] M. F. Karim, A. Q. Alphones, and A. B. Yu, "A novel reconfigurable filter using periodic structures," in *IEEE MTT-S Int. Microw. Symp. Dig.*, San Francisco, CA, 2006, pp. 9343–946.
[12] Y.-M. Chen, S.-F. Chang, C.-Y. Chou, and K.-H. Liu, "A reconfigurable bandpass-bandstop filter based on varactor-loaded closed-ring resonators," *IEEE Microw. Mag.*, vol. 10, no. 1, pp. 138–140, Feb. 2009.
[13] S. Amari and U. Rosenberg, "New building blocks for modular design of elliptic and self-equalized filters," *IEEE Trans. Microw. Theory Techn.*, vol. 52, no. 2, pp. 721–736, Feb. 2004.
[14] E. J. Naglich, J. Lee, D. Peroulis, and W. J. Chappell, "High-Q tunable bandstop filters with adaptable bandwidth and pole allocation," in *IEEE MTT-S Int. Microw. Symp. Dig.*, Baltimore, MD, 2011, pp. 1–4.
[15] R. J. Cameron, C. M. Kudsia, and R. R. Mansour, *Microwave Filters for Communications Systems: Fundamentals, Design, and Applications*. Hoboken, NJ: Wiley, 2007.
[16] N. Marcuvitz, *Waveguide Handbook*. Stevenage, U.K.: Peregrinus, 1993.
[17] E. J. Naglich, J. Lee, D. Peroulis, and W. J. Chappell, "Extended passband bandstop filter cascade with continuous 0.85–6.6-GHz coverage," *IEEE Trans. Microw. Theory Techn.*, vol. 60, no. 1, pp. 21–30, Jan. 2012.
[18] D. Kajfez and P. Guillon, *Dielectric Resonators*. Norwood, MA: Artech House, 1986.
[19] R. S. Kwok and J.-F. Liang, "Characterization of high-Q resonators for microwave-filter applications," *IEEE Trans. Microw. Theory Techn.*, vol. 47, no. 1, pp. 111–114, Jan. 1999.
[20] C.-S. Ahn, J. Lee, and Y.-S. Kim, "Design flexibility of an open-loop resonator filter using similarity transformation of coupling matrix," *IEEE Microw. Wireless Compon. Lett.*, vol. 15, no. 4, pp. 262–264, Apr. 2005.

Juseop Lee (A'02–M'03) received the B.E. and M.E. degrees in radio science and engineering from Korea University, Seoul, Korea, in 1997 and 1999, respectively, and the Ph.D. degree in electrical engineering from The University of Michigan at Ann Arbor, in 2009.

In 1999, he joined LG Information and Communications (now LG Electronics), where his activities included design and reliability analysis of RF components for code-division multiple-access (CDMA) cellular systems. In 2001, he joined the Electronics and Telecommunications Research Institute (ETRI), where he was involved in designing passive microwave equipment for Ku- and Ka-band communications satellites. In 2005, he joined The University of Michigan at Ann Arbor, where he was a Research Assistant and Graduate Student Instructor with the Radiation Laboratory, and his research activities focused on millimeter-wave radars and synthesis techniques for multiple-passband microwave filters. In 2009, he joined Purdue University, West Lafayette, IN, where he was a Post-Doctoral Research Associate, and his activities included the design of adaptable RF systems. In 2012, he joined Korea University, Seoul, Korea, where he is currently an Assistant Professor. His research interests include RF and microwave components, satellite transponders, wireless power transfer, and EM theories.

Dr. Lee was a recipient of the Freshman Award presented by Korea University, the Undergraduate Fellowship presented by Korea University, the Graduate Fellowship presented by LG Information and Communications, the Graduate Fellowship presented by the Korea Science and Engineering Foundation, the Rackham Predoctoral Fellowship presented by Rackham Graduate School, The University of Michigan at Ann Arbor, and the IEEE Microwave Theory and Techniques Society (IEEE MTT-S) Graduate Fellowship. He coauthored a paper in the 2010 IEEE MTT-S International Microwave Symposium (IMS) Student Paper Competition, which received the 2nd Place Award. He is listed in *Who's Who in America*.

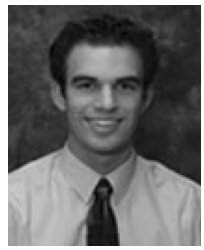

Eric J. Naglich (S'09) received the B.S.E.C.E. degree from Purdue University, West Lafayette, IN, in 2007, and is currently working toward the Ph.D. degree in electrical and computer engineering at Purdue University.

From 2007 to 2009, he was with GE Healthcare, where he was involved with EM subsystem design in medical imaging and surgical navigation machines during the Edison Engineering Development Program. His current research focuses on tunable filter synthesis and fabrication for widely tunable, adaptive RF front ends in cognitive radio and radar applications.

Mr. Naglich is a National Defense Science and Engineering Graduate (NDSEG) Fellow. He is a member of the IEEE Microwave Theory and Techniques Society (IEEE MTT-S). He is a past president of Purdue University's MTT-S Student Chapter and Beta Chapter of Eta Kappa Nu. He coauthored a paper in the 2010 IEEE MTT-S International Microwave Symposium (IMS) Student Paper Competition, which received the 2nd Place Award. His project received the 2nd Place Award in the 2012 IEEE MTT-S IMS Power Amplifier Student Competition.

Hjalti H. Sigmarsson (S'01–M'10) received the B.S.E.C.E. degree from the University of Iceland, Reykjavik, Iceland, in 2003, and the M.S.E.C.E. and Ph.D. degrees in electrical and computer engineering from Purdue University, West Lafayette, IN, in 2005 and 2010, respectively.

He is currently an Assistant Professor with the School of Electrical and Computer Engineering, University of Oklahoma, Norman, where he teaches EM field theory, circuit theory, and advanced filter design and synthesis. He is a member of the Advanced Radar Research Center (ARRC). His current research focuses on reconfigurable RF and microwave hardware for agile communications, measurement, and radar systems. His research interests further include spectral management schemes for cognitive radio architectures and advanced packaging utilizing heterogeneous integration techniques.

Dr. Sigmarsson is a member of the IEEE Microwave Theory and Techniques Society (IEEE MTT-S) and the International Microelectronics and Packaging Society (IMAPS). He was the recipient of the Best Paper Award of IMAPS 2008 41st International Symposium on Microelectronics.

Dimitrios Peroulis (S'99–M'04) received the Ph.D. degree in electrical engineering from The University of Michigan at Ann Arbor, in 2003.

Since August 2003, he has been with Purdue University, where he currently leads a group of graduate students on a variety of research projects in the areas of RF MEMS, sensing and power harvesting applications, as well as RF identification (RFID) sensors for the health monitoring of sensitive equipment. He has been a Principal Investigator (PI) or a co-PI of numerous projects funded by government agencies and industry in these areas. He has been a key contributor on developing very high quality ($Q > 1000$) RF MEMS tunable filters in mobile form factors. Furthermore, he has been investigating failure modes of RF MEMS and MEMS sensors through the Defense Advanced Research Projects Agency (DARPA) MEMS/nanoelectromechanical systems (NEMS) Science and Technology Fundamentals Program, Phases I and II) and the Center for the Prediction of Reliability, Integrity and Survivability of Microsystems (PRISM) funded by the National Nuclear Security Administration. He was the recipient of the National Science Foundation CAREER Award in 2008. His students have been the recipients of numerous Student Paper Awards and other student research-based scholarships. He is a Purdue University Faculty Scholar and has been the recipient of ten teaching awards, including the 2010 HKN C. Holmes MacDonald Outstanding Teaching Award and the 2010 Charles B. Murphy Award, which is Purdue University's highest undergraduate teaching honor.

William J. Chappell (S'98–M'02–SM'09) received the B.S.E.E., M.S.E.E., and Ph.D. degrees from The University of Michigan at Ann Arbor, in 1998, 2000, and 2002, respectively.

He is currently an Associate Professor with the School of Electrical and Computer Engineering, Purdue University, West Lafayette, IN, where he is also a Member of the Birck Nanotechnology Center and the Center for Wireless Systems and Applications. His research focus is on advanced applications of RF and microwave components. He has been involved with numerous Defense Advanced Research Projects Agency (DARPA) projects involved in advanced packaging and material processing for microwave applications. His research sponsors include HSARPA, the Office of Naval Research (ONR), the National Science Foundation (NSF), the State of Indiana, Communications–Electronics Research, Development and Engineering Center (CERDEC), and the Army Research Office (ARO), as well as industry sponsors. His research group uses EM analysis, unique processing of materials, and advanced design to create novel microwave components. His specific research interests are the application of very high-quality and tunable components utilizing multilayer packages. In addition, he is involved with high-power RF systems, packages, and applications.

Dr. Chappell was the IEEE Microwave Theory and Techniques Society (IEEE MTT-S) Administrative Committee (AdCom) secretary for 2009 and was elected to the IEEE MTT-S AdCom for 2010–2012.